Covert Beamforming Design for Active RIS-Assisted NOMA-ISAC Systems

Pengxu Chen*, Fengcheng Xiao*, Liang Yang†, Theodoros A. Tsiftsis‡, and Hongwu Liu*
* School of Information Science and Electrical Engineering, Shandong Jiaotong University, Jinan 250357, China
† College of Computer Science and Electronic Engineeing, Hunan University, Changsha 410082, China
‡ Department of Informatics and Telecommunications, University of Thessaly, 35100 Lamia, Greece
Email: 21208019@stu.sdjtu.edu.cn, 21208017@stu.sdjtu.edu.cn, liangy@hnu.edu.cn, tsiftsis@uth.gr, liuhongwu@sdjtu.edu.cn

2023 IEEE Globecom Workshops (GC Wkshps) | 979-8-3503-7021-8/23/$31.00 ©2023 IEEE | DOI: 10.1109/GCWKSHPS58843.2023.10464669

***Abstract*—In this paper, an active reconfigurable intelligent surface (RIS) is deployed to assist covert communications in a non-orthogonal multiple access (NOMA) inspired integrated sensing and communication (ISAC) system. With the aid of the active RIS, a dual-function base-station (BS) serves a public user and a covert user under the NOMA principles while sensing multiple targets by using the superimposed sensing and communication signal. To maximize the covert rate of the NOMA-inspired ISAC (NOMA-ISAC) system, transmission beamforming at BS and reflection beamforming at active RIS are jointly optimized subject to QoS requirements of the NOMA public user, sensing beampattern similarity constraint, and covertness level against the warden. To tackle the optimization variables coupled in the objective function and constraints, an alternating optimization algorithm is proposed, while the resulted non-convex fractional programming subproblems of transmission and reflection beamforming optimizations are solved by exploiting a penalized Dinkelbach transformation to obtain a high-quality rank-one solution. Numerical results demonstrate that the active RIS-assisted NOMA-ISAC scheme outperforms the passive RIS-assisted counterpart in terms of the covert rate and sensing beampattern similarity.**

***Index Terms*—Active reconfigurable intelligent surface (RIS), covert beamforming design, integrated sensing and communication (ISAC)**

I. Introduction

With expanding of communication bandwidths and developments of multiple-input multiple-output (MIMO) techniques, waveforms are now suitable for radar target sensing at a reasonable range resolution [1]. Toward this trend, the concept of integrated sensing and communication (ISAC) has recently sparked heated discussions, particularly on the design of dual-functional waveforms [1]–[3]. Compared to orthogonal multiple access (OMA), non-orthogonal multiple access (NOMA) seems to be a viable solution for supporting multicast transmission and mitigating inter-user interference in NOMA-inspired ISAC (NOMA-ISAC) systems with limited wireless resources [4]. By adequately designing transmission beamforming, the superimposed NOMA signal can be exploited for guaranteeing an effective sensing quality while maximizing the communication throughput [5]. With the aid of successive interference cancellation (SIC), the transmit powers of the communication and sensing waveforms were well-designed in NOMA-ISAC systems, which ensures an accurate radar sensing and provides a new degree of freedom (DoF) for communications. However, due to the open and broadcasting natures of NOMA-ISAC systems, the sensitive and privacy information embedded in waveforms is susceptible to interception and eavesdropping in the presence of malicious users.

A novel technology known as reconfigurable intelligent surface (RIS) has been developed to reflect wireless signal constructively or destructively, such that the arrived signal power on the desired directions can be strengthened or weakened by smartly adjusting the reflecting amplitudes and phase shifts [6]. Due to this property, RIS is often utilized to facilitate covert communications in NOMA systems [7], [8], which provides a higher level of security than the conventional physical layer security (PLS) by endeavoring to conceal the legitimate transmissions against wardens. Compared to covert communications in NOMA systems, where only the signal of the NOMA public user was utilized as a shield for covert transmissions [9], RIS-aided superposition transmissions can cost-effectively hide covert communication behaviors by leveraging the RIS's phase shift uncertainties and the non-orthogonal transmissions of the NOMA public user. Nevertheless, the reflecting link quality of the passive RIS-aided wireless communication system is limited due to the effect of "multiplicative fading", leading to a negligible capacity gain. To overcome this limitation, the active RIS was proposed [10], [11]. The active RIS integrated amplifiers into the meta-elements to amplify the reflected signals, compensating for the substantial path loss of reflected links and obviating the need for complex and power-hungry radio frequency (RF) chain components at the base-station (BS) [10]. With the aid of the active RIS, the performance of PLS [12] and covert communication [13] can be improved by optimizing reflection beamforming at the active RIS and collaborating with the BS transmission optimization.

Although PLS has been studied in NOMA-ISAC systems to improve the secure performance [14], emerging researches are needed on covert communications for NOMA-ISAC systems with the aim of achieving a higher security level. On the other hand, active RIS has not yet been applied to assist covert communications in NOMA-ISAC systems and how to exploit reflection beamforming to improve the covert communication performance for NOMA-ISAC systems is still unknown. Motivated by the above observations, we propose to deploy an active RIS to assist covert communications in a NOMA-ISAC system. In the considered NOMA-ISAC system, both

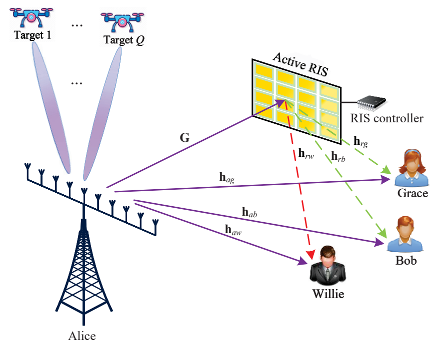

Fig. 1. The Active RIS-assisted NOMA-ISAC System Model.

the sensing signal and NOMA public user's signal are utilized as the covert medium to hide covert transmissions from the dual-function BS to the NOMA covert user. Moreover, the active RIS's reflection beamforming is exploited to provide the additional covert rate gain with less transmit power, which allows allocating additional transmit power for target sensing. To maximize the covert rate, the transmission beamforming at the BS and the reflection beamforming of the active RIS are jointly optimized, subject to the NOMA QoS constraint, power budget constraints at the BS and active RIS, beampattern similarity constraint, and covertness constraint. Specifically, we decouple the non-convex covert rate maximization problem into two sub-problems of the BS's transmission beaforming and the active RIS's reflection beamforming, respectively, and propose an alternating optimization (AO) algorithm to optimize the transmission and reflection beamforming in an alternating manner. Taking into account the non-convex fractional characteristics of the decoupled sub-problems, a penalized Dinkelbach transform approach is proposed to achieve the high-quality rank-one solutions. Numerical results demonstrate that the active RIS-assisted NOMA-ISAC system outperforms the passive RIS-assisted counterpart in terms of the covert rate and sensing beampattern similarity.

II. System Model

We consider an active RIS-assisted NOMA-ISAC system consisting of an NOMA-ISAC BS (Alice), an active RIS, a warden (Willie), a NOMA public user (Grace), a NOMA covert user (Bob), and Q point-like targets indexed by $\mathcal{Q} = \{1, ..., Q\}$, as depicted in Fig. 1. In the NOMA-ISAC system, Alice is equipped with a uniform linear array (ULA) with M transmit/receive antennas. Grace, Bob, and Willie are respectively equipped with a single antenna. The active RIS consists of N reflecting elements and is deployed close to the users to assist covert communications. We assume that the targets fly at low altitudes, which results in the strong line of sight (LoS) links from the targets to Alice and vice versa, while the active RIS is deployed far away from the targets resulting in the weak RIS reflection links. Thus, we only consider the direct links for the target sensing [3]. In addition, Willie keeps monitoring the communication behaviors from Alice to the NOMA users and determining whether Alice is transmitting covert information to Bob. The link between Alice and node k is denoted by $\mathbf{h}_{ak} \in \mathbb{C}^{M\times 1}$ with $k = g$, b, and w standing for Grace, Bob, and Willie, respectively. The Alice-RIS link and RIS-k link are denoted by $\mathbf{G} \in \mathbb{C}^{N\times M}$ and $\mathbf{h}_{rk} \in \mathbb{C}^{N\times 1}$, respectively. Similar to works in [7], [8], we assume that Alice knows statistical channel state information (CSI) of the links associated with Willie and perfect CSI of the remaining channels. Willie acquires perfect CSI of its monitoring channels. All the channels are assumed to experience quasi-static block fading and maintain constant state within a block.

A. Signal Model

To serve two NOMA users and sense the targets simultaneously, Alice transmits the superimposed NOMA and sensing signal in each transmission block, which is given by

$$\mathbf{x} = \mathbf{W}_c\mathbf{s}_c + \mathbf{W}_s\mathbf{s}_s = \mathbf{W}\mathbf{s}, \tag{1}$$

where $\mathbf{s}_c = [s_g, s_b]^T \in \mathbb{C}^{2\times 1}$ denotes the NOMA symbols satisfying $\mathbb{E}\{\mathbf{s}_c\mathbf{s}_c^H\} = \mathbf{I}_2$, s_b and s_g are the message signals for Bob and Grace, respectively, $\mathbf{s}_s \in \mathbb{C}^{M\times 1}$ is the sensing signal satisfying $\mathbb{E}\{\mathbf{s}_s\mathbf{s}_s^H\} = \mathbf{I}_M$, $\mathbf{W}_c \triangleq [\mathbf{w}_g, \mathbf{w}_b] \in \mathbb{C}^{M\times 2}$ is the communication beamforming matrix with $\mathbf{w}_i \in \mathbb{C}^{M\times 1}$ denoting the beamforming vector for s_i ($\forall i \in \{g, b\}$), and $\mathbf{W}_s \in \mathbb{C}^{M\times M}$ is the sensing beamforming matrix. In (1), $\mathbf{W}$ is the overall beamforming matrix given by $\mathbf{W} \triangleq [\mathbf{W}_c, \mathbf{W}_s] \in \mathbb{C}^{M\times(2+M)}$ and $\mathbf{s} = [\mathbf{s}_c^T, \mathbf{s}_s^T]^T \in \mathbb{C}^{(2+M)\times 1}$. Furthermore, we assume that the sensing signal is independent of the NOMA symbols.

In each transmission block, the transmitted signal from Alice arrives at the active RIS and then it is reflected by the active RIS. Taking into account the additive noise at the active RIS, the reflected signal can be written as:

$$\mathbf{y}_r = \mathbf{\Phi}\mathbf{G}\mathbf{x} + \mathbf{\Phi}\mathbf{z}_r, \tag{2}$$

where $\mathbf{\Phi} \in \mathbb{C}^{N\times N}$ is a $N \times N$ diagonal matrix with its nth diagonal entity $\mathbf{\Phi}_{n,n}$ denoting the reflection coefficient of the nth element of the active RIS and $\mathbf{z}_r \sim \mathcal{CN}\left(\mathbf{0}, \sigma_r^2\mathbf{I}_N\right)$ denotes the additive noise at the active RIS. Specifically, $|\mathbf{\Phi}_{n,n}| \le \eta_n$ and $\arg(\mathbf{\Phi}_{n,n}) \in [0, 2\pi)$ respectively represent the reflecting amplitude and phase shift the nth element and $\eta_n > 1$ is the allowed maximum reflecting amplitude. The total power of the reflected signal is limited by

$$\|\mathbf{\Phi}\mathbf{G}\mathbf{W}\|_F^2 + \|\mathbf{\Phi}\|_F^2\sigma_r^2 \le P_r^{\max}, \tag{3}$$

where $P_r^{\max}$ is the maximum power budget at the active RIS. Then, the received signal at node k, $k \in \{g, b, w\}$, can be expressed as:

$$y_k = \mathbf{g}_k^H\mathbf{x} + \mathbf{h}_{rk}^H\mathbf{\Phi}\mathbf{z}_r + z_k, \tag{4}$$

where $\mathbf{g}_k^H = \mathbf{h}_{ak}^H + \mathbf{h}_{rk}^H\mathbf{\Phi}\mathbf{G}$ is the equivalent composite channel from Alice to node k and $z_k \sim \mathcal{CN}\left(0, \sigma_b^2\right)$ is the additive noise at node k. With the assumption that $\|\mathbf{g}_b\|^2 \ge \|\mathbf{g}_g\|^2$, i.e., Bob and Grace are the near and far users, respectively, Alice allocates more transmit power to transmit s_g rather than s_b, i.e., $\|\mathbf{w}_g\|^2 > \|\mathbf{w}_b\|^2$, to guarantee the successfully SIC. According to the NOMA principles, Bob first detects s_g

and removes the corresponding interference by exploiting SIC followed by the detection of its own signal s_b, while treating the sensing signal as noise. Grace detects s_g by treating the signals related to s_b and $\mathbf{s}_s$ as noise. In this paper, we assume that the sensing signal cannot be cancelled by Bob and Grace. Then, the achievable rates of Bob corresponding to the transmissions of s_g and s_b are given by $R_{b,s_g} = \log_2(1+\gamma_{b,s_g})$ and $R_{b,s_b} = \log_2(1+\gamma_{b,s_b})$, respectively, with

$$\gamma_{b,s_g} = \frac{|\mathbf{g}_b^H \mathbf{w}_g|^2}{|\mathbf{g}_b^H \mathbf{w}_b|^2 + \|\mathbf{g}_b^H \mathbf{W}_s\|^2 + \|\mathbf{h}_{rb}^H \mathbf{\Phi}\|^2 \sigma_r^2 + \sigma_b^2} \tag{5}$$

and

$$\gamma_{b,s_b} = \frac{\left|\mathbf{g}_b^H \mathbf{w}_b\right|^2}{\|\mathbf{g}_b^H \mathbf{W}_s\|^2 + \|\mathbf{h}_{rb}^H \mathbf{\Phi}\|^2 \sigma_r^2 + \sigma_b^2}. \tag{6}$$

Furthermore, the achievable rate of Grace is given by

$$R_{g,s_g} = \log_2\left(1+\frac{|\mathbf{g}_g^H \mathbf{w}_g|^2}{|\mathbf{g}_g^H \mathbf{w}_b|^2 + \|\mathbf{g}_g^H \mathbf{W}_s\|^2 + \|\mathbf{h}_{rg}^H \mathbf{\Phi}\|^2 \sigma_r^2 + \sigma_g^2}\right). \tag{7}$$

The monitoring of Willie involves two hypotheses: $\mathcal{H}_0$ indicates the absence of the covert transmission from Alice to Bob, and $\mathcal{H}_1$ indicates the occurrence of the covert transmission from Alice to Bob. Under $\mathcal{H}_0$ and $\mathcal{H}_1$, the received signals at Willie can be respectively expressed as:

$$\mathcal{H}_0: \ y_w = \mathbf{g}_w^H (\mathbf{w}_g s_g + \mathbf{W}_s \mathbf{s}_s) + \mathbf{h}_{rw}^H \mathbf{\Phi} \mathbf{z}_r + z_w \tag{8}$$

and

$$\mathcal{H}_1: \ y_w = \mathbf{g}_w^H \mathbf{x} + \mathbf{h}_{rw}^H \mathbf{\Phi} \mathbf{z}_r + z_w. \tag{9}$$

B. Covertness Requirement

Assuming Willie uses the Neyman-Pearson criterion to detect the covert transmission, the optimal decision rule for minimizing the detection error probability (DEP) is the likelihood ratio test, i.e.,

$$\frac{p_1(y_w)}{p_0(y_w)} \underset{\mathcal{D}_0}{\overset{\mathcal{D}_1}{\gtrless}} 1, \tag{10}$$

where $\mathcal{D}_0$ and $\mathcal{D}_1$ denote Willie's binary decisions endorsing $\mathcal{H}_0$ and $\mathcal{H}_1$, respectively, $p_0(y_w) = \frac{1}{\pi\sigma_0^2} e^{-|y_w|^2/\sigma_0^2}$ and $p_1(y_w) = \frac{1}{\pi\sigma_1^2} e^{-|y_w|^2/\sigma_1^2}$ denote the likelihood functions for Willie's received signals under $\mathcal{H}_0$ and $\mathcal{H}_1$, respectively, with $\sigma_0^2 = |\mathbf{g}_w^H \mathbf{w}_g|^2 + \|\mathbf{g}_w^H \mathbf{W}_s\|^2 + \left\|\mathbf{h}_{rw}^H \mathbf{\Phi}\right\|^2 \sigma_r^2 + \sigma_w^2$ and $\sigma_1^2 = \|\mathbf{g}_w^H \mathbf{W}\|^2 + \|\mathbf{h}_{rw}^H \mathbf{\Phi}\|^2 \sigma_r^2 + \sigma_w^2$, respectively. With respect to Willie's received signal power, the optimal decision rule for Willie can be rewritten as:

$$P_w \underset{\mathcal{D}_0}{\overset{\mathcal{D}_1}{\gtrless}} \phi^*, \tag{11}$$

where $P_w \overset{L\to\infty}{=} \frac{1}{L}\sum_{l=1}^{L} |y_w(l)|^2$ with l denoting the index of the transmission block and $\phi^* = \frac{\sigma_0^2\sigma_1^2}{\sigma_0^2-\sigma_1^2} \ln \frac{\sigma_1^2}{\sigma_0^2} > 0$ denotes the chosen optimal detection threshold. With the optimal detection rule, we can derive the minimum DEP achieved by Willie under the two hypotheses as [15]:

$$\begin{aligned}\xi^* &= \Pr(\mathcal{D}_1|\mathcal{H}_0) + \Pr(\mathcal{D}_1|\mathcal{H}_1) \\ &= 1 + \left(\frac{\sigma_1^2}{\sigma_0^2}\right)^{-\frac{\sigma_1^2}{\sigma_1^2-\sigma_0^2}} - \left(\frac{\sigma_1^2}{\sigma_0^2}\right)^{-\frac{\sigma_0^2}{\sigma_1^2-\sigma_0^2}},\end{aligned} \tag{12}$$

where $\Pr(\mathcal{D}_1|\mathcal{H}_0)$ and $\Pr(\mathcal{D}_0|\mathcal{H}_1)$ denote the probabilities of false alarm and missed detection, respectively. To facilitate the design of covert communications, we introduce a lower bound on ξ^* [15]:

$$\xi^* \geq 1 - \sqrt{\frac{1}{2}\mathcal{D}(p_0(y_w)||p_1(y_w))}, \tag{13}$$

where $\mathcal{D}(p_0(y_w)||\, p_1(y_w))$ refers to the Kullback-Leibler (KL) divergence, which can be calculated as follows:

$$\mathcal{D}(p_0(y_w)||p_1(y_w)) = \ln\left(\frac{\sigma_1^2}{\sigma_0^2}\right) + \frac{\sigma_0^2}{\sigma_1^2} - 1. \tag{14}$$

To ensure covertness, the minimum DEP of Willie should satisfy $\xi^* \geq 1-\varepsilon$, where $\varepsilon > 0$ is the desired level of covertness. In this work, we set a tighter constraint $\mathcal{D}(p_0(y_w)|p_1(y_w)) \leq 2\varepsilon^2$ to ensure covertness, taking into account the lower bound on ξ^* in (13). According to (14), by applying the monotonicity of the function $f(\lambda) = \ln\lambda + \frac{1}{\lambda} - 1$ in the interval $[1,\infty)$, the covertness constraint can be reformulated as follows:

$$\begin{aligned}|\mathbf{g}_w^H \mathbf{w}_b|^2 + (1-\kappa)\Big(|\mathbf{g}_w^H \mathbf{w}_g|^2 + \|\mathbf{g}_w^H \mathbf{W}_s\|^2 + \|\mathbf{h}_{rw}^H \mathbf{\Phi}\|^2 \sigma_r^2\Big) \\ \leq (\kappa-1)\sigma_w^2,\end{aligned} \tag{15}$$

where κ is the unique root of $f(\lambda) = 2\varepsilon^2$ in the interval $[1,\infty)$.

C. Sensing Requirement

In the NOMA-ISAC system, the transmitted NOMA signal can be exploited for target sensing [4]. In this work, we consider the beampattern similarity as the metric for evaluating the sensing performance by comparing the designed beampattern with the desired one [3]. Let $\mathbf{a}(\theta) = [1, e^{j2\pi\delta\sin(\theta)}, ..., e^{j2\pi(M-1)\delta\sin(\theta)}]^T$ denote the transmit/receive steering vector at the direction θ with δ being the normalized antenna spacing. We define the transmit beampattern $P(\theta)$ as the transmit signal power distribution at the direction angle, which is given by [3]

$$P(\theta) = \mathbb{E}\{|\mathbf{a}^H(\theta)\mathbf{W}\mathbf{x}|^2\} = \mathbf{a}^H(\theta)\mathbf{W}\mathbf{W}^H\mathbf{a}(\theta). \tag{16}$$

The mean squared error (MSE) of the beampattern matching is used to evaluate the beampattern similarity, which measures the difference between the actual transmission beampattern and the desired beampattern, i.e.,

$$\mathcal{E}(\alpha,\mathbf{W}) \triangleq \frac{1}{V}\sum_{v=1}^{V} \left|\alpha\hat{P}(\theta_v) - \mathbf{a}^H(\theta_v)\mathbf{W}\mathbf{W}^H\mathbf{a}(\theta_v)\right|^2. \tag{17}$$

In (17), θ_v denotes the vth sampled angle over $[-\frac{\pi}{2}, \frac{\pi}{2}]$, α is a scaling factor and $\hat{P}(\theta_v)$ is the desired beampattern defined as a square waveform at the target direction $\hat{\theta}_q$, i.e.,

$$\hat{P}(\theta_v) = \begin{cases} 1, & \exists q \in \mathcal{Q},\ |\theta_v - \hat{\theta}_q| < \frac{\Delta\theta}{2}, \\ 0, & \text{otherwise}, \end{cases} \tag{18}$$

where $\hat{\theta}_q$ denotes the direction of the qth target and $\Delta\theta$ denotes the width of desired beampattern at each estimation angle.

III. Covert Beamforming Design

The aim of the covert beamforming design is to maximize the covert rate R_{b,s_b} by jointly optimizing the transmission beamforming and reflection beamforming, subject to the power budget constraints of Alice and active RIS, Grace's QoS requirement, sensing beampattern similarity requirement, and pre-defined covertness level. Considering the additional constraints imposed by the NOMA-ISAC system, the covert rate maximization problem is formulated as follows:

$$\text{(P1)}: \max_{\alpha,\mathbf{W},\mathbf{\Phi}} R_{b,s_b} \tag{19a}$$
$$\text{s.t.}\ \ \|\mathbf{W}\|_F^2 \le P_a^{\max}, \tag{19b}$$
$$R_{g,s_g} \le R_{b,s_g},\ \|\mathbf{w}_g\|^2 \ge \|\mathbf{w}_b\|^2, \tag{19c}$$
$$R_{g,s_g} \ge R_g^{\min}, \tag{19d}$$
$$\frac{1}{V}\sum_{v=1}^{V}\left|\alpha\hat{P}(\theta_v) - \mathbf{a}^H(\theta_v)\mathbf{W}\mathbf{W}^H\mathbf{a}(\theta_v)\right|^2 \le \epsilon, \tag{19e}$$
$$|\mathbf{\Phi}_{n,n}| \le \eta_n,\ (3),\ (15). \tag{19f}$$

In problem (P1), (19b) is Alice's maximum transmit power constraint, (19c) guarantees successful SIC at Bob, (19d) ensures that Grace achieves the minimum target rate $R_g^{\min}$ to meet its QoS requirements, (19e) guarantees the desired beampattern similarity, and constraints in (19f) denote the limitations of the maximum reflecting amplitude of nth element of $\mathbf{\Phi}$, reflection power budget at the active RIS, and covertness level, respectively. However, due to the coupling between the optimization variables $\mathbf{W}$ and $\mathbf{\Phi}$ in problem (P1), the joint optimization of $\mathbf{W}$ and $\mathbf{\Phi}$ is infeasible. To address this challenge, we propose to decouple problem (P1) into two sub-problems of optimizing the transmission beamforming and reflection beamforming, respectively. Considering that maximizing R_{b,s_b} is equivalent to maximizing γ_{b,s_b}, we drop the $\log(\cdot)$ function and propose a penalized Dinkelbach approach to recast the resulting non-convex fractional programming (FP) sub-problems with rank-one constraints to a convex form. Furthermore, we design an AO algorithm to maximize the covert rate. The details of our proposed scheme are presented in the following subsections.

A. Transmission Beamforming Optimization

For any given feasible $\mathbf{\Phi}$, problem (P1) can be reduced to optimize $\mathbf{W}$ only. To facilitate solving the covert rate maximization problem, we introduce the auxiliary variables $\mathbf{W}_i = \mathbf{w}_i\mathbf{w}_i^H$, $i \in \{g,b\}$, $\tilde{\mathbf{W}}_s = \mathbf{W}_s\mathbf{W}_s^H$, $\mathbf{\Upsilon}_k = \mathbf{g}_k\mathbf{g}_k^H$, $\mathbf{H}_{rk} = \mathbf{h}_{rk}\mathbf{h}_{rk}^H$, $\mathbf{\Psi} = \mathbf{\Phi}\mathbf{\Phi}^H$ and $\mathbf{\Gamma} = \bar{\mathbf{\Gamma}}^H\bar{\mathbf{\Gamma}}$ with $\bar{\mathbf{\Gamma}} = \mathbf{\Phi}\mathbf{G}$. One can obtain that $\left|\mathbf{g}_k^H\mathbf{w}_i\right|^2 = \mathrm{tr}(\mathbf{\Upsilon}_k\mathbf{W}_i)$, $\left\|\mathbf{g}_k^H\mathbf{W}_s\right\|^2 = \mathrm{tr}(\mathbf{\Upsilon}_k\tilde{\mathbf{W}}_s)$, $\|\mathbf{h}_{rk}^H\mathbf{\Phi}\|^2 = \mathrm{tr}(\mathbf{H}_{rk}\mathbf{\Psi})$, and $\|\mathbf{\Phi}\mathbf{G}\mathbf{W}\|_F^2 + \|\mathbf{\Phi}\|_F^2\sigma_r^2 = \mathrm{tr}(\mathbf{\Gamma}\tilde{\mathbf{W}}) + \mathrm{tr}(\mathbf{\Psi})\sigma_r^2$ with $\tilde{\mathbf{W}} = \mathbf{W}_g + \mathbf{W}_b + \tilde{\mathbf{W}}_s$. After dropping the $\log(\cdot)$ function, the optimization problem with respect to $\mathbf{W}$ can be formulated as:

$$\text{(P2)}: \max_{\alpha,\mathbf{W}_g,\mathbf{W}_b,\tilde{\mathbf{W}}_s} \frac{\mathrm{tr}(\mathbf{\Upsilon}_b\mathbf{W}_b)}{\mathrm{tr}(\mathbf{\Upsilon}_b\tilde{\mathbf{W}}_s)+\mathrm{tr}(\mathbf{H}_{rb}\mathbf{\Psi})\sigma_r^2+\sigma_b^2} \tag{20a}$$
$$\text{s.t.}\ \ \mathrm{tr}(\tilde{\mathbf{W}}) \le P_a^{\max},\ \mathrm{tr}(\mathbf{W}_g) \ge \mathrm{tr}(\mathbf{W}_b), \tag{20b}$$
$$\gamma_{\text{th}}\Big(\mathrm{tr}\big(\mathbf{\Upsilon}_g(\mathbf{W}_b+\tilde{\mathbf{W}}_s)\big)+\mathrm{tr}(\mathbf{H}_{rg}\mathbf{\Psi})\sigma_r^2+\sigma_g^2\Big) \le \mathrm{tr}(\mathbf{\Upsilon}_g\mathbf{W}_g), \tag{20c}$$
$$\frac{1}{V}\sum_{v=1}^{V}\left|\alpha\hat{P}(\theta_v) - \mathbf{a}^H(\theta_v)\tilde{\mathbf{W}}\mathbf{a}(\theta_v)\right|^2 \le \epsilon, \tag{20d}$$
$$\mathrm{tr}(\mathbf{\Gamma}\tilde{\mathbf{W}}) + \mathrm{tr}(\mathbf{\Psi})\sigma_r^2 \le P_r^{\max}, \tag{20e}$$
$$\mathrm{tr}(\mathbf{\Upsilon}_w\mathbf{W}_b)+(1-\kappa)\Big(\mathrm{tr}\big(\mathbf{\Upsilon}_w(\mathbf{W}_g+\tilde{\mathbf{W}}_s)\big)+\mathrm{tr}(\mathbf{H}_{rw}\mathbf{\Psi})\sigma_r^2\Big) \le (\kappa-1)\sigma_w^2, \tag{20f}$$
$$\mathbf{W}_g \succeq 0,\ \mathbf{W}_b \succeq 0,\ \tilde{\mathbf{W}}_s \succeq 0, \tag{20g}$$
$$\mathrm{rank}(\mathbf{W}_g) = 1,\ \mathrm{rank}(\mathbf{W}_b) = 1, \tag{20h}$$

In problem (P2), constraint (20c) represents the QoS requirements of Grace with $\gamma_{\text{th}} = 2^{R_g^{\min}} - 1$. To address the rank-one constraint (20h), we introduce a penalty term $\frac{1}{\iota_1}\sum_{i\in\{g,b\}}\big(\|\mathbf{W}_i\|_* + \widehat{\mathbf{W}}_i^{(t)}\big)$ in the denominator of (20a), where ι_1 is a penalty factor, $\|\cdot\|_*$ denotes the nuclear norm, and $\widehat{\mathbf{W}}_i^{(t)}$ is the convex upper bound of the non-convex term $-\|\mathbf{W}_i\|_2$ with $\|\cdot\|_2$ standing for the spectral norm, i.e., $-\|\mathbf{W}_i\|_2 \le \widehat{\mathbf{W}}_i^{(t)}$. Here, if $\iota_1 \to 0$, the exactly rank-one metrics can be guaranteed by maximizing the fractional objective function due to the fact $\mathrm{rank}(\mathbf{W}_i) = 1$ is equivalent to $\|\mathbf{W}_i\|_* - \|\mathbf{W}_i\|_2 = 0$. One can obtain the convex upper bound $\widehat{\mathbf{W}}_i^{(t)}$ by leveraging the first-order Taylor expansion at the point $\mathbf{W}_i^{(t)}$, which is expressed as $\widehat{\mathbf{W}}_i^{(t)} \triangleq -\|\mathbf{W}_i^{(t)}\|_2 - \mathrm{tr}[\mathbf{q}_{\max,i}^{(t)}(\mathbf{q}_{\max,i}^{(t)})^H(\mathbf{W}_i - \mathbf{W}_i^{(t)})]$, where $\mathbf{W}_i^{(t)}$ is the solution obtained in the tth iteration and $\mathbf{q}_{\max,i}^{(t)}$ is the eigenvector corresponding to the largest eigenvalue of $\mathbf{W}_i^{(t)}$. With the added penalty term, the objective function of problem (P2) is expressed as:

$$\frac{\mathrm{tr}(\mathbf{\Upsilon}_b\mathbf{W}_b)}{\mathrm{tr}(\mathbf{\Upsilon}_b\tilde{\mathbf{W}}_s)+\mathrm{tr}(\mathbf{H}_{rb}\mathbf{\Psi})\sigma_r^2+\sigma_b^2+\frac{1}{\iota_1}\sum\limits_{i\in\{g,b\}}\Big(\|\mathbf{W}_i\|_*+\widehat{\mathbf{W}}_i^{(k)}\Big)}. \tag{21}$$

Since the above single-ratio concave-convex fractional objective function still hinders a direct solution, we further utilize the Dinkelbach transformation [16] to convert it into a concave form. In particular, by defining $f_1(\mathbf{W}_b) = \mathrm{tr}(\mathbf{\Upsilon}_b\mathbf{W}_b)$, and $f_2(\tilde{\mathbf{W}}_s,\mathbf{W}_i) = \mathrm{tr}(\mathbf{\Upsilon}_b\tilde{\mathbf{W}}_s) + \mathrm{tr}(\mathbf{H}_{rb}\mathbf{\Psi})\sigma_r^2 + \sigma_b^2 + \frac{1}{\iota_1}\sum\limits_{i\in\{g,b\}}(\|\mathbf{W}_i\|_* + \widehat{\mathbf{W}}_i^{(k)})$, we obtain the following transformed optimization problem:

$$\text{(P2.1)}: \max_{\alpha,\mathbf{W}_g,\mathbf{W}_b,\tilde{\mathbf{W}}_s} f_1(\mathbf{W}_b) - u_1 f_2(\tilde{\mathbf{W}}_s,\mathbf{W}_i) \tag{22a}$$
$$\text{s.t.}\ \ (20b)-(20g), \tag{22b}$$

where the auxiliary variable u_1 achieves the optimal value when $u_1^{(\ell+1)} = f_1^{(\ell)}(\mathbf{W}_b)/f_2^{(\ell)}(\tilde{\mathbf{W}}_s,\mathbf{W}_i)$ in the ℓth iteration. It is evident that problem (P2.1) is a convex optimization problem and can be readily solved using existing convex optimization solvers such as CVX.

B. Reflection Beamforming Optimization

For any given $\mathbf{W}$, problem (P1) can be reduced to optimize $\mathbf{\Phi}$ only. To handle the non-convexity of the objective function and constraints (19c), (19d), and (19f) with respect to $\mathbf{\Phi}$ and formulate a tractable covert rate maximization problem, we first introduce $\bar{\mathbf{u}} = [\phi_1, \ldots, \phi_N]$ with ϕ_n, $\forall n \in \{1, \ldots, N\}$, being the n-th diagonal element in $\mathbf{\Phi}$ and $\bar{\mathbf{\Lambda}}_{k,j} = [\mathrm{diag}(\mathbf{h}_{rk}^H)\mathbf{G}\mathbf{w}_j; \mathbf{h}_{ak}^H\mathbf{w}_j]$ with $\mathbf{w}_j$ bing the jth, $j \in \{1, ..., 2+M\}$, column of the beamforming matrix $\mathbf{W}$ and construct $\mathbf{\Lambda}_{k,j} = \bar{\mathbf{\Lambda}}_{k,j}\bar{\mathbf{\Lambda}}_{k,j}^H$ and $\mathbf{U} = \mathbf{u}\mathbf{u}^H$ with $\mathbf{u} = [\bar{\mathbf{u}}, 1]^H$, which results in the expression $\left|\mathbf{g}_k^H\mathbf{w}_j\right|^2 = \mathrm{tr}(\mathbf{\Lambda}_{k,j}\mathbf{U})$. Then, by applying the change of variables $\mathbf{\Omega}_k = \mathrm{diag}\left(|[\mathbf{h}_{rk}]_1|^2, ..., |[\mathbf{h}_{rk}]_N|^2, 0\right)$, $\mathbf{\Pi} = \mathrm{diag}([\mathbf{1}_{1\times N}, 0]^T)$, and $\mathbf{S}_j = \mathrm{diag}\left(|[\mathbf{s}_j]_1|^2, ..., |[\mathbf{s}_j]_N|^2, 0\right)$ with $\mathbf{s}_j = \mathbf{G}\mathbf{w}_j$, we obtain that $\|\mathbf{\Phi}\mathbf{G}\mathbf{W}\|_F^2 = \sum_{j=1}^{2+M}\mathrm{tr}(\mathbf{S}_j\mathbf{U})$, $\|\mathbf{h}_{rk}^H\mathbf{\Phi}\|^2 = \mathrm{tr}(\mathbf{\Omega}_k\mathbf{U})$, and $\|\mathbf{\Phi}\|_F^2 = \mathrm{tr}(\mathbf{\Pi}\mathbf{U})$. After taking the ratio term γ_{b,s_b} out of the $\log(\cdot)$ function, we can formulate the reflection beamforming optimization problem as:

$$\text{(P3)}: \quad \max_{\mathbf{U}} \ \frac{\mathrm{tr}(\mathbf{\Lambda}_{b,2}\mathbf{U})}{\sum_{j=3}^{2+M}\mathrm{tr}(\mathbf{\Lambda}_{b,j}\mathbf{U}) + \mathrm{tr}(\mathbf{\Omega}_b\mathbf{U})\sigma_r^2 + \sigma_b^2} \tag{23a}$$

$$\text{s.t.} \quad \mathrm{tr}(\mathbf{\Lambda}_{g,1}\mathbf{U}) \le \mathrm{tr}(\mathbf{\Lambda}_{b,1}\mathbf{U}), \tag{23b}$$

$$\mathrm{tr}(\mathbf{\Lambda}_{g,1}\mathbf{U}) \ge \gamma_{\mathrm{th}}\left(\sum_{j=2}^{2+M}\mathrm{tr}(\mathbf{\Lambda}_{g,j}\mathbf{U}) + \mathrm{tr}(\mathbf{\Omega}_g\mathbf{U})\sigma_r^2 + \sigma_g^2\right), \tag{23c}$$

$$\sum_{j=1}^{2+M}\mathrm{tr}(\mathbf{S}_j\mathbf{U}) + \mathrm{tr}(\mathbf{\Pi}\mathbf{U})\sigma_r^2 \le P_r^{\max}, \tag{23d}$$

$$\mathrm{tr}(\mathbf{\Lambda}_{w,2}\mathbf{U}) + (1-\kappa)\left(\sum_{j=1, j\neq 2}^{2+M}\mathrm{tr}(\mathbf{\Lambda}_{w,j}\mathbf{U}) + \mathrm{tr}(\mathbf{\Omega}_w\mathbf{U})\sigma_r^2\right) \le (\kappa - 1)\sigma_w^2, \tag{23e}$$

$$|\mathbf{U}_{n,n}| \le \eta_n^2, \ \forall n, \ |\mathbf{U}_{N+1,N+1}| = 1, \tag{23f}$$

$$\mathrm{rank}(\mathbf{U}) = 1, \ \mathbf{U} \succeq 0. \tag{23g}$$

Similar to the approach adopted in (21), we add a penalty-term $\frac{1}{\iota_2}(\|\mathbf{U}\|_* + \widehat{\mathbf{U}}^{(t)})$ to the objection function's denominator to address the non-convexity of rank-1 constraint generated by variable changes in (23g). Here, ι_2 is a control factor, and $\widehat{\mathbf{U}}^{(t)}$ is the upper bound on $-\|\mathbf{U}\|_2$ with closed form $\widehat{\mathbf{U}}^{(t)} = -\|\mathbf{U}\|_2^{(t)} - \mathrm{tr}\big(\mathbf{u}_{\max}^{(t)}(\mathbf{u}_{\max}^{(t)})^H(\mathbf{U} - \mathbf{U}^{(t)})\big)$, where $\mathbf{u}_{\max}^{(t)}$ represents the eigenvector corresponding to the largest eigenvalue of $\mathbf{U}^{(t)}$ in the tth solution. As a result, the new objective function can be expressed as:

$$\frac{\mathrm{tr}(\mathbf{\Lambda}_{b,2}\mathbf{U})}{\sum_{j=3}^{2+M}\mathrm{tr}(\mathbf{\Lambda}_{b,j}\mathbf{U}) + \mathrm{tr}(\mathbf{\Omega}_b\mathbf{U})\sigma_r^2 + \sigma_b^2 + \frac{1}{\iota_2}\left(\|\mathbf{U}\|_* + \widehat{\mathbf{U}}^{(t)}\right)}. \tag{24}$$

By maximizing this fractional objective function, we ensure that $\mathrm{rank}(\mathbf{U}) = 1$ as $\iota_2 \to 0$, as $\|\mathbf{U}\|_* - \|\mathbf{U}\|_2 = 0$ is equivalent to $\mathrm{rank}(\mathbf{U}) = 1$. Since the concave-convex single-ratio objective in (24) still hinders a direct solution, we apply the Dinkelbach transformation to convert it into a concave form. Specifically, let $f_3(\mathbf{U}) = \mathrm{tr}(\mathbf{\Lambda}_{b,2}\mathbf{U})$ and $f_4(\mathbf{U}) = \sum_{j=3}^{2+M}\mathrm{tr}(\mathbf{\Lambda}_{b,j}\mathbf{U}) + \mathrm{tr}(\mathbf{\Omega}_b\mathbf{U})\sigma_r^2 + \sigma_b^2 + \frac{1}{\iota_2}\left(\|\mathbf{U}\|_* + \widehat{\mathbf{U}}^{(t)}\right)$, the transformed optimization problem can be expressed as:

Algorithm 1 AO Algorithm for Optimizing $\mathbf{W}$ and $\mathbf{U}$

Initialize $s \leftarrow 0$, $\mathbf{U}^{(0)}$ and $\mathbf{W}^{(0)}$
repeat $s \leftarrow s + 1$
    $t \leftarrow 0$
    repeat $t \leftarrow t + 1$
        Initialize $u_1^{(0)} > 0$, $\ell \leftarrow 0$
        repeat $\ell \leftarrow \ell + 1$
            Update $\mathbf{W}^{(\ell)}$ by solving (P2.1)
            Update $u_1^{(\ell+1)} = f_1^{(\ell)}(\mathbf{W}_b)/f_2^{(\ell)}(\tilde{\mathbf{W}}_s, \mathbf{W}_i)$
        until $f_1^{(\ell)}(\mathbf{W}_b) - u_1^{(\ell)} f_2^{(\ell)}(\tilde{\mathbf{W}}_s, \mathbf{W}_i) \le 0$
        $\mathbf{W}^{(t)} \leftarrow \mathbf{W}^{(\ell)}$, $\iota_1 \leftarrow c_1\iota_1$
    until $\frac{1}{\iota_1}\sum_{i\in\{g,b\}}(\|\mathbf{W}_i\|_* + \widehat{\mathbf{W}}_i^{(t)}) \le \xi_3$
    $\mathbf{W}^{(s)} \leftarrow \mathbf{W}^{(t)}$
    $t \leftarrow 0$
    repeat $t \leftarrow t + 1$
        Initialize $u_2^{(0)} > 0$, $\ell \leftarrow 0$
        repeat $\ell \leftarrow \ell + 1$
            Update $\mathbf{U}^{(\ell)}$ by solving (P3.1)
            Update $u_2^{(\ell+1)} = f_3^{(\ell)}(\mathbf{U})/f_4^{(\ell)}(\mathbf{U})$
        until $f_3^{(\ell)}(\mathbf{U}) - u_2^{(\ell)} f_4^{(\ell)}(\mathbf{U}) \le 0$
        $\mathbf{U}^{(t)} \leftarrow \mathbf{U}^{(\ell)}$, $\iota_2 \leftarrow c_2\iota_2$
    until $\frac{1}{\iota_2}(\|\mathbf{U}\|_*^{(t)} + \widehat{\mathbf{U}}^{(t)}) \le \xi_2$
    $\mathbf{U}^{(s)} \leftarrow \mathbf{U}^{(t)}$
until $R_{b,s_b}^{(s)} - R_{b,s_b}^{(s-1)} \le \xi_1$

$$\text{(P3.1)}: \ \max_{\mathbf{U}} \ f_3(\mathbf{U}) - u_2 f_4(\mathbf{U}) \tag{25a}$$

$$\text{s.t. (23b), (23c), (23d), (23e), (23f)}, \ \mathbf{U} \succeq \mathbf{0}, \tag{25b}$$

where the auxiliary variable u_2 is updated by $u_2^{(\ell+1)} = f_3^{(\ell)}(\mathbf{U})/f_4^{(\ell)}(\mathbf{U})$ in the ℓth iteration. Now, problem (P3.1) is convex, $\mathbf{U}$ can be optimized via existed CVX solver.

The proposed AO algorithm is summarized in Algorithm 1. To prevent the optimization falling into local optima caused by the zero penalty-term during initialization, we set $u^{(0)} > 0$ in the proposed penalized Dinkelbach approach. The overall computational complexity of Algorithm 1 is characterized by $\mathcal{O}\left[I_{\mathrm{A}}(I_{\mathrm{P}_1}I_{\mathrm{D}}(3M^{3.5}) + I_{\mathrm{P}_2}I_{\mathrm{D}}(N+1)^{3.5})\right]$, where I_{A} and I_{D} denote the iteration numbers of the AO loop and Dinkelbach loop, respectively, and I_{P_1} and I_{P_2} denote the iteration numbers of the penalty-terms in problems (P2.1) and (P3.1), respectively.

IV. Numerical Results

Numerical results are provided in this section to validate the system performance of the active RIS-assisted NOMA-ISAC system. In the simulations, we set $M = 8$, $N = 16$, $\sigma_b^2 = \sigma_g^2 = \sigma_w^2 = \sigma_r^2 = -90$ dBm, $R_g^{\min} = 1$ bps/Hz, $\eta_n^2 = \eta^2$, $\forall n$, $c_1 = c_2 = \xi_1 = 10^{-2}$, $\xi_2 = \xi_2 = 10^{-4}$, $\Delta\theta = 10°$, and $Q = 3$ with the targets located in $\hat{\theta}_1 = -35°$, $\hat{\theta}_2 = 0°$, and $\hat{\theta}_3 = 35°$, respectively. Alice, Bob, Grace, Willie, and active RIS are located at $(0, 0)$ m, $(80, 10)$ m, $(90, 0)$ m, $(100, 5)$ m, and $(80, 30)$ m, respectively, in a two-dimensional coordinate space. The path-loss is modeled by $\mathcal{L} = \mathcal{L}_0 d^{-\chi}$ with $\mathcal{L}_0 = -30$ dB and d denoting the distance between the two terminals. We set $\chi = 3.5$ for the direct links and $\chi = 2.2$ for the channels associated with the active RIS [12].

In Fig. 2, we plot an example of the optimal transmit beampattern $P(\theta)$ achieved by the proposed algorithm versus the azimuth angle over $[-90°, 90°]$ for a single Monte Carlo realization. The passive RIS scheme is also presented as

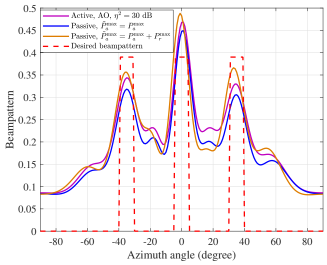

Fig. 2. Transmit beampattern ($P_a^{\max} = 30$ dBm, $P_r^{\max} = 30$ dBm, $\varepsilon = 0.1$)

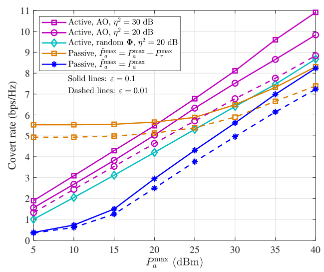

Fig. 3. Covert rate versus transmit power ($P_r^{\max} = 30$ dBm)

the benchmark. We consider two scenarios for the passive RIS scheme where Alice has a power budget of either $\tilde{P}_a^{\max} = P_a^{\max}$ or $\tilde{P}_a^{\max} = P_a^{\max} + P_r^{\max}$ for comparison. The curves of Fig. 2 show that the passive RIS scheme with $\tilde{P}_a^{\max} = P_a^{\max} + P_r^{\max}$ achieves a higher beampattern compared with the active RIS scheme, which is quite predicted owing to the availability of the total transmit power budget at Alice. However, the active RIS scheme has a more preferred shape than the passive RIS scheme when the transmit power budget is the same. It is verified that deploying the active RIS to assist communications in the NOMA-ISAC system can save more transmit power of Alice for target sensing, thereby obtaining better sensing performance than the passive RIS scheme.

In Fig. 3, we investigate the impact of the maximum transmit power budget on the covert rate in different schemes when $P_r^{\max} = 30$ dBm. In addition to the passive RIS scheme, we also compare the covert rate achieved by the proposed AO algorithm to the random $\mathbf{\Phi}$ scheme of the active RIS. The curves in Fig. 3 reveal that the passive RIS scheme with $\tilde{P}_a^{\max} = P_a^{\max} + P_r^{\max}$ achieves a higher covert rate than the active RIS scheme in the low transmit power region, while the active RIS scheme performs better with the increasing of $P_a^{\max}$. The active RIS scheme always outperforms the passive RIS scheme with $\tilde{P}_a^{\max} = P_a^{\max}$ even through applying a random reflection beamforming. Additionally, the curves in Fig. 3 also confirm that a higher η^2 leads to a higher covert rate when $P_r^{\max}$ remains constant. The proposed active RIS-assisted NOMA-ISAC system can achieve a considerable covert rate in the high transmit power region mainly thanks to the additional covert rate gain of the active RIS and the shield of the NOMA public user's signal and sensing signal.

V. Conclusions

In this paper, we have designed the AO-optimized covert beamforming to maximize the covert rate for the active RIS-assisted NOMA-ISAC system. The penalized Dinkelbach approach has been proposed to achieve the high-quality rank-one solutions for the decoupled sub-problems of the transmission and reflection beamforming with non-convex fractional characteristics. The numerical results have verified the superiority of the proposed AO algorithm. The significant advantages of deploying active RIS in the NOMA-ISAC system have also been demonstrated in terms of the covert rate and sensing beampattern similarity.

Acknowledgments

This work was supported in part by the National Natural Science Foundation of China under Grant 62071202 and in part by the Shandong Provincial Natural Science Foundation under Grant ZR2020MF009. Corresponding author: Hongwu Liu.

References

[1] F. Liu, L. Zhou, C. Masouros, A. Li, W. Luo, and A. Petropulu, "Toward dual-functional radar-communication systems: Optimal waveform design," *IEEE Trans. Signal Process.*, vol. 66, no. 16, pp. 4264–4279, Aug. 2018.

[2] R. Liu, M. Li, Q. Liu, and A. L. Swindlehurst, "Dual-functional radar-communication waveform design: A symbol-level precoding approach," *IEEE J. Sel. Topics Signal Process.*, vol. 15, no. 6, pp. 1316–1331, Nov. 2021.

[3] H. Luo, R. Liu, M. Li, Y. Liu, and Q. Liu, "Joint beamforming design for RIS-assisted integrated sensing and communication systems," *IEEE Trans. Veh. Technol.*, vol. 71, no. 12, pp. 13 393–13 397, 2022.

[4] X. Mu, Y. Liu, L. Guo, J. Lin, and L. Hanzo, "NOMA-aided joint radar and multicast-unicast communication systems," *IEEE J. Select. Areas Commun.*, vol. 40, no. 6, pp. 1978–1992, Jun. 2022.

[5] Z. Wang, Y. Liu, X. Mu, Z. Ding, and O. A. Dobre, "NOMA empowered integrated sensing and communication," *IEEE Commun. Lett.*, vol. 26, no. 3, pp. 677–681, Mar. 2022.

[6] X. Tan, Z. Sun, J. M. Jornet, and D. Pados, "Increasing indoor spectrum sharing capacity using smart reflect-array," in *Proc. 2016 IEEE Int. Conf. Commun. (ICC)*, Kuala Lumpur, Malaysia, 22-27 May 2016, pp. 1–6.

[7] L. Lv, Q. Wu, Z. Li, Z. Ding, N. Al-Dhahir, and J. Chen, "Covert communication in intelligent reflecting surface-assisted NOMA systems: Design, analysis, and optimization," *IEEE Trans. Wireless Commun.*, vol. 21, no. 3, pp. 1735–1750, 2022.

[8] L. Yang, W. Zhang, P. S. Bithas, H. Liu, M. O. Hasna, T. A. Tsiftsis, and D. W. K. Ng, "Covert transmission and secrecy analysis of RS-RIS-NOMA-aided 6G wireless communication systems," *IEEE Trans. Veh. Technol.*, pp. 1–12, 2023.

[9] Y. Zhang, W. He, X. Li, H. Peng, K. Rabie, G. Nauryzbayev, B. M. ElHalawany, and M. Zhu, "Covert communication in downlink NOMA systems with channel uncertainty," *IEEE Sensors J.*, vol. 22, no. 19, pp. 19 101–19 112, 2022.

[10] R. Long, Y.-C. Liang, Y. Pei, and E. G. Larsson, "Active reconfigurable intelligent surface-aided wireless communications," *IEEE Trans. Wireless Commun.*, vol. 20, no. 8, pp. 4962–4975, Aug. 2021.

[11] K. Zhi, C. Pan, H. Ren, K. K. Chai, and M. Elkashlan, "Active RIS versus passive RIS: Which is superior with the same power budget?" *IEEE Commun. Lett.*, vol. 26, no. 5, pp. 1150–1154, 2022.

[12] L. Dong, H.-M. Wang, and J. Bai, "Active reconfigurable intelligent surface aided secure transmission," *IEEE Trans. Veh. Technol.*, vol. 71, no. 2, pp. 2181–2186, 2022.

[13] M. Wang, Z. Xu, B. Xia, and Y. Guo, "Active intelligent reflecting surface assisted covert communications," *IEEE Trans. Veh. Technol.*, vol. 72, no. 4, pp. 5401–5406, 2023.

[14] Z. Yang, D. Li, N. Zhao, Z. Wu, Y. Li, and D. Niyato, "Secure precoding optimization for NOMA-aided integrated sensing and communication," *IEEE Trans. Commun.*, vol. 70, no. 12, pp. 8370–8382, 2022.

[15] B. A. Bash, D. Goeckel, and D. Towsley, "Limits of reliable communication with low probability of detection on AWGN channels," *IEEE J. Sel. Areas Commun.*, vol. 31, no. 9, pp. 1921–1930, Sep. 2013.

[16] W. Dinkelbach, "On nonlinear fractional programming," *Management Science*, vol. 13, no. 7, pp. 492–498, 1967.